

# One-Step Generation of Core–Gap–Shell Microcapsules for Stimuli-Responsive Biomolecular Sensing

Hyejeong Kim,\* Seong-Min Jo, Fanlong Meng, Yinzhou Guo, Héloïse Thérien-Aubin, Ramin Golestanian, Katharina Landfester, and Eberhard Bodenschatz

The versatile design of stimuli-responsive microparticles embedding valuable biomolecules has great potential in a variety of engineering fields, such as sensors, actuators, drug delivery, and catalysis. Here, results are reported on thermoresponsive core–gap–shell (TCGS) microcapsules made of poly(*N*-isopropylacrylamide) (PNIPAM), which encapsulate hydrophilic payloads in a simple and stable manner. These are realized by a one-step microfluidic approach using the phase separation of a supersaturated aqueous solution of NIPAM. Various designs of the microcapsules are achieved by individual control of the swelling or by incorporating pH-responsive comonomers of the inner core and outer shell. The gap, i.e., the space between the inner core and outer shell, can be loaded with cargo-like nanoparticles. The outer shell can serve as a stimuli-responsive gateway for the transport of smaller molecules from the external solution. It is shown that the TCGS microcapsules are suitable as temperature controllable glucose sensors and hold promise in the design of controllable enzymatic reactions. The proposed platform provides an avenue for developing a new-generation of microparticles for diverse and efficient engineering applications.

## 1. Introduction

Droplet microfluidics can produce microdroplets with precisely tunable configurations at high throughput.<sup>[1]</sup> Recent advances in microfluidics have established multiple-emulsion technologies, which allow the fabrication of microcapsules with a membrane (block copolymers, lipids, etc.) with possible applications to, for example, biomedicine, foods, and cosmetics.<sup>[1a,b,d,2]</sup> Microcapsules, also termed microcompartments, are promising candidates for the building of proto-cells in bottom-up synthetic biology.<sup>[3]</sup> For microcapsules to be versatile, they must be able to encapsulate cargo materials stably. Recently, perfluoropolyether-based double emulsion drops,<sup>[4]</sup> nanosensors encapsulating poly(ethylene glycol) (PEG) microcapsules,<sup>[5]</sup> PEG diacrylate-based microcapsules,<sup>[6]</sup> and fluorocarbon oil-reinforced triple emulsion drops<sup>[7]</sup> have been used to encapsulate a broad range of cargoes

in a single platform. To date, it is still a challenge to fabricate water-cored capsules dispersed in aqueous media that enable to encapsulate hydrophilic biomolecules.<sup>[1c,8]</sup> In addition, the sophistication needed in production limits bulk production for commercial-scale manufacturing.<sup>[1d,9]</sup> In particular, in order to produce stable and uniform multilayer droplets, the microchannel geometry and wettability, as well as the flow rates in the individual multichannels need to be precisely controlled to achieve uniform microcapsules with homogeneous geometry, which is why most scale-up studies restrict themselves to the production of a single-emulsion.<sup>[10]</sup>

Stimuli-responsive microparticles are excellent candidates for functional units in a variety of engineering applications, such as sensors, actuators, drug delivery, and catalysis.<sup>[8b,11]</sup> Under the various external stimuli, the shell of microparticles passively undergoes mechanical deformation or chemical reactions. This enables the effective delivery of valuable and sensitive cargo in response to external field triggers. They allow controllable transport of biomolecules to target locations, where they are delivered by direct environmental changes.<sup>[8a,11a,c,12]</sup> However, due to the lack of methods for producing aqueous-cored microcapsules, the encapsulation of hydrophilic cargoes within stimuli-responsive microcapsules is currently limited to pH-responsive anhydride microcapsules with an aqueous core.<sup>[8b,c,13]</sup> One alternative material for the production of stimuli-responsive microcapsules is the thermoresponsive polymer, poly(*N*-isopropylacrylamide) (PNIPAM). This polymer collapses or swells by tuning the temperature

Dr. H. Kim, Dr. F. Meng, Dr. H. Thérien-Aubin, Prof. R. Golestanian, Prof. K. Landfester, Prof. E. Bodenschatz  
Max Planck—University of Twente Center for Complex Fluid Dynamics  
University of Twente  
Drienerlolaan 5, 7522, NB Enschede, The Netherlands  
E-mail: hyejeong.kim@ds.mpg.de

Dr. H. Kim, Dr. F. Meng, Prof. R. Golestanian, Prof. E. Bodenschatz  
Max Planck Institute for Dynamics and Self-Organization  
Am Faßberg 17, 37077 Göttingen, Germany

Dr. S.-M. Jo, Y. Guo, Dr. H. Thérien-Aubin, Prof. K. Landfester  
Max Planck Institute for Polymer Research  
Ackermannweg 10, 55128 Mainz, Germany

Prof. E. Bodenschatz  
Institute for the Dynamics of Complex Systems  
Georg-August-University Göttingen  
37073 Göttingen, Germany

Prof. E. Bodenschatz  
Laboratory of Atomic and Solid-State Physics and Sibley School  
of Mechanical and Aerospace Engineering  
Cornell University  
Ithaca, New York 14853, USA

 The ORCID identification number(s) for the author(s) of this article can be found under <https://doi.org/10.1002/adfm.202006019>.

© 2020 The Authors. Published by Wiley-VCH GmbH. This is an open access article under the terms of the Creative Commons Attribution License, which permits use, distribution and reproduction in any medium, provided the original work is properly cited.

DOI: 10.1002/adfm.202006019

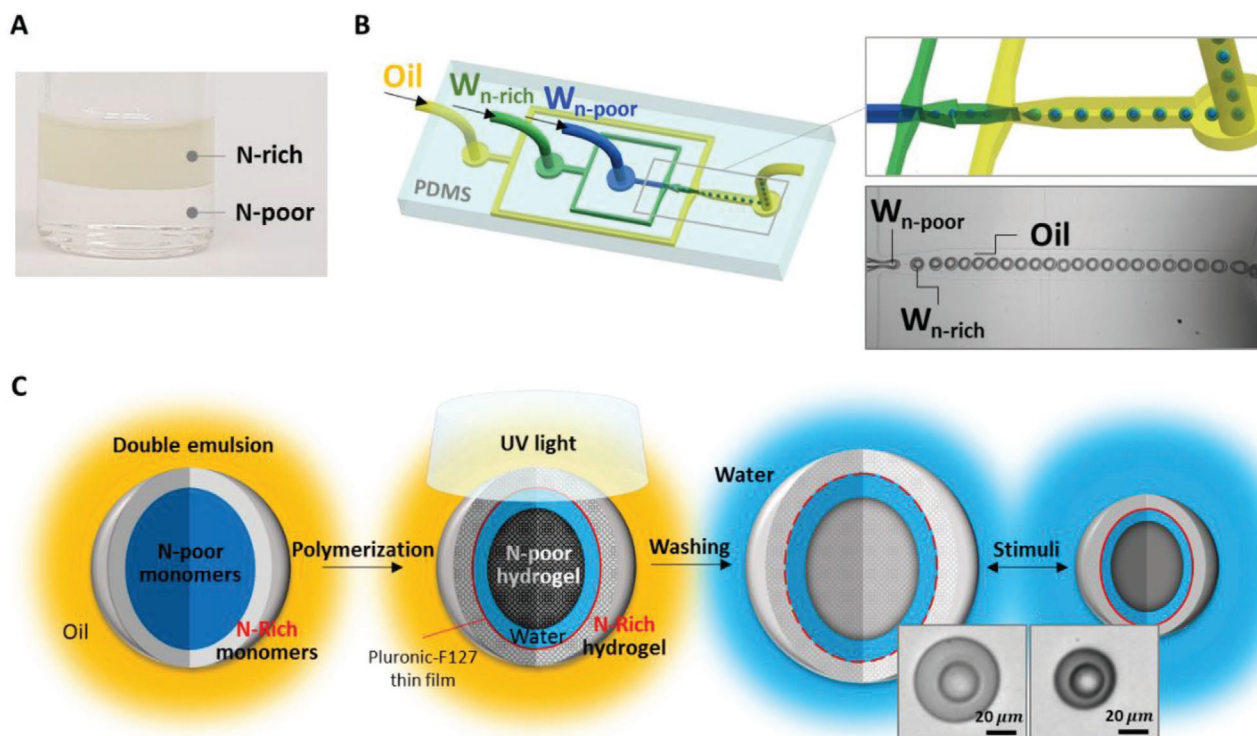


**Figure 1.** Formation of core–gap–shell microcapsule. A) Supersaturated NIPAm solution is separated into two immiscible phases at 25 °C; one is an oleophilic NIPAm-rich (N-rich) phase and the other is a hydrophilic NIPAm-poor (N-poor) phase. B) With  $W_{n-poor}$ ,  $W_{n-rich}$  solutions as inlet fluids into an oil,  $W_{n-poor}/W_{n-rich}/O$  double emulsion droplets are generated in microfluidic device. C) Schematic illustration showing the strategy for the synthesis of TCGS microcapsules. Double emulsion droplets are polymerized with UV radiation generating a microcapsule with an N-rich hydrogel shell, an inner aqueous solute gap, and an N-poor hydrogel core in the middle. After polymerization, the oil is removed by washing with isopropanol and water. Depending on the condition of the external solution, the microcapsule is reversibly shrunk/swollen by extrusion/absorption of water molecules.

above or below the lower critical solution temperature (LCST) of 32 °C. PNIPAm microparticles have been designed to be potentially used for temperature triggered release or loading actives at the target location.<sup>[14]</sup> By incorporating NIPAm with other monomers, the resulting copolymerized microparticles have been made to sense specific ions or molecules, such as organic acid, glucose, and heavy metals, and to sense other physical stimuli, such as light and magnetic fields.<sup>[14a,15]</sup> However, as NIPAm is water-soluble, it cannot be used as a shell material to directly encapsulate water-based bioactive materials. In consequence, so far, PNIPAm microparticles have found almost no application in complex chemical and biomedical applications, such as enzymatic reactions or chain reactions.<sup>[11c,16]</sup>

Here, we report a microfluidic approach to produce temperature-responsive core–gap–shell (TCGS) microcapsules that enable the encapsulation of hydrophilic nanoparticles in a straightforward manner. Our approach relies on using an oleophilic phase of supersaturated NIPAm solution as the base material for the outer shell of the microcapsules, allowing the encapsulation of hydrophilic payloads in the diluted NIPAm phase. We demonstrate the design variability of the TCGS platform for multifunctional microcapsules by adjusting the water absorption ability and incorporating the pH-responsive copolymer. In addition, we demonstrate the direct loading of aqueous-dispersed polystyrene nanoparticles inside the microcapsules during the formation of the double emulsion templates. If the use of organic solvents for oil-phase washing during the manu-

facturing process can be avoided, for example by slowly hydrolyzing the oil-phase,<sup>[13b]</sup> our platform could be used efficiently in synthetic biology for encapsulating sensitive biological samples such as antibodies, viruses, and cells. As a more practical application, we develop and demonstrate a controllable enzymatic reactor as a glucose sensor. We realize this by successfully encapsulating glucose oxidase-loaded silica nanocontainers (GOX@nanocontainers) inside the microcapsules. Controlled diffusion of glucose by temperature allows regulating enzymatic reaction kinetics. A numerical diffusion-reaction model well represents the experimental results, as well as is helpful to describe the mass transport inside the capsule. Thus the TCGS microcapsules are excellent candidates for a versatile platform of microcapsules, particularly for on-demand chemical reactions.

## 2. Results and Discussion

### 2.1. Formation of TCGS Microcapsules

By leveraging the thermodynamic properties of supersaturated NIPAm solution, TCGS microcapsules can be produced from  $W_{n-poor}/W_{n-rich}/O$  double emulsions generated from a polydimethylsiloxane (PDMS) microfluidic device (**Figure 1**). Supersaturated NIPAm solution separates into two immiscible phases at temperatures above 25 °C; one phase,  $W_{n-rich}$ , is NIPAm-rich (N-rich) and oleophilic (hydrophobic) and the other,  $W_{n-poor}$  is

NIPAm-poor (N-poor) and hydrophilic (Figure 1A).<sup>[17]</sup> NIPAm is an amphiphilic material possessing a hydrophilic amide group and a hydrophobic isopropyl group. To be dissolved in aqueous solution, the hydrophobic isopropyl group of NIPAm needs to be hydrated, which is called hydrophobic hydration. The N-poor phase has more than 20 H<sub>2</sub>O molecules surrounding each NIPAm molecule.<sup>[17a,18]</sup> On the other hand, the N-rich phase has each NIPAm molecule surrounded roughly only by one H<sub>2</sub>O molecule. Thus, in the N-rich solution, the majority of the hydrophobic isopropyl group are not hydrated and the solution exhibits hydrophobicity. When polymerized, both monomer solutions formed a PNIPAm hydrogel.

$W_{n-poor}$  and  $W_{n-rich}$  pregel solutions were used in the microfluidic channel as inner fluid and middle fluid, respectively (Figure 1B).  $W_{n-poor}/W_{n-rich}/O$  double emulsions were successfully generated without any chemical treatment of the channel surface.<sup>[18]</sup> With the help of surfactants, Pluronic F-127 (PF-127) in  $W_{n-poor}$  and Span 80 in  $W_{n-rich}$ , pregel solutions of  $W_{n-poor}$  and  $W_{n-rich}$  could be well separated and diffusion between two phases was negligible. Depending on the interfacial tensions between the three liquid phases, the droplet configuration is determined; nonengulfing, complete engulfing, or partial engulfing configurations.<sup>[19]</sup> For the complete engulfing configuration, where the droplet of  $W_{n-poor}$  phase is entirely encapsulated by the  $W_{n-rich}$  phase, the relationship of  $(\gamma_{W_{n-poor}-rich} > \gamma_{W_{n-rich}-rich} + \gamma_{W_{n-poor}-rich, W_{n-rich}})$  should be satisfied, where  $\gamma_{A,B}$  is an interfacial force between the A phase and the B phase. The topology and stability of the  $W_{n-poor}/W_{n-rich}/O$  double emulsion droplets are controlled by varying the interfacial tensions between the immiscible three phases using the proper concentration of surfactants to each (Figures S3 and S5, Supporting Information).<sup>[20]</sup>

Once the double emulsions of microdroplets were formed, they were polymerized and crosslinked by UV irradiation (Figure 1C). While polymerization proceeded in the presence of covalent crosslinker, *N,N*-methylenebisacrylamide (MBAm), PF-127 formed very thin polymer films at the interface of the  $W_{n-poor}$  and  $W_{n-rich}$  solutions, creating distinct compartmentalized structures of core and shell in a single synthetic step (Figure S1A–C, Supporting Information). In the case of  $W_{n-poor}$  solution polymerization, the volume of the droplet decreased as polymerization proceeded, while the thin-film of PF-127 polymer remained in the initial template shapes (Figure S1D, Supporting Information). As a result, completely separated inner core and outer shell were formed with a thin membrane of PF-127 at the interface (Figure 1C; Figure S1E, Supporting Information). By increasing the temperature from 25 to 40 °C, the microcapsule expelled water and shrunk.

Our platform, a microfluidic approach to produce TCGS microcapsules using a phase separated of NIPAm solution, increases the production yield of stable microcapsule templates by reducing the order of emulsions. In previous studies, core-gap-shell (CGS) microcapsules are generally fabricated from triple-emulsions, where each layer has alternating polarity with an adjacent layer.<sup>[1b]</sup> The advantages of our platform can be more advantageous when the number of target layers of microcapsules increases. In other methods, as the order of emulsion is increased, smaller drops contained in a higher order of emulsion tend to coalesce before the emulsion drops are converted into stabilized capsules.<sup>[21]</sup> Our approach avoids coalescence, thus increases the yield of stable microcapsules.

## 2.2. Design Variability of the Microcapsule

### 2.2.1. Varying the Degree of Swelling

TCGS structure is flexible and allows various functional designs by varying chemical compositions in the separated inner phase and middle phase of double emulsions templates. For instance, the water absorption ability of the inner core and outer shell can be individually controlled by adding different amounts of crosslinker. To investigate the effect of crosslinker concentration on water absorption behavior, we prepared microparticles with different amounts of crosslinker composition from a single emulsion (Figure 2A; Table S1, Supporting Information). When both  $W_{n-poor}$  and  $W_{n-rich}$  solutions have the same concentration of crosslinker, the N-rich particle has much larger swelling ratio than an N-poor particle (Figure 2B). This different tendency of water absorption ability is due to different NIPAm/H<sub>2</sub>O mole ratio of  $W_{n-poor}$  and  $W_{n-rich}$  solutions. It is reported that the value of NIPAm/H<sub>2</sub>O mole ratio for the N-rich solution is about 0.77, and that of N-poor solution is roughly around 0.04 at 25 °C.<sup>[17a]</sup> Even with the same amount of crosslinker, the larger quantity of NIPAm in the N-rich solution will result in fewer crosslinking point per unit of volume, thereby giving a higher swelling ratio.<sup>[22]</sup>

By combining the different composition of the N-poor inner fluid and N-rich outer fluid, TCGS microcapsules with different water absorption capabilities can be fabricated (Figure 2C). The water absorption capacity of the core can be controlled depending on the degree of volume shrinkage of the shell which wraps the core. To demonstrate this controlled shrinkage, two different kinds of microcapsules were formed; the first one had a loosely crosslinked N-poor P2 (N-poor solution containing 2 mg of crosslinker) core surrounded by a moderately crosslinked N-rich R10 (N-rich solution containing 10 mg of crosslinker) outer shell (Figure 2C-a) and another had the same P2 core surrounded by a heavily crosslinked R30 (N-rich solution containing 30 mg of crosslinker) outer shell (Figure 2C-b). The chemical composition of each solution is denoted in Table S1 in the Supporting Information. Even though both inner cores are made of the same P2 solution, the swelling ratio of the core depends on the crosslinking of the outer shell which surrounds the core (Figure 2C-c; Figure S4, Supporting Information). When the pure P2 microparticle is independently shrunken by heating, the swelling ratio is  $0.1 \pm 0.07$  on average. When the P2 inner core is surrounded by the R30 outer shell, whose average swelling ratio is  $0.13 \pm 0.03$ , the swelling ratio of the P2 inner core is  $0.09 \pm 0.03$ , almost the same as that of single emulsion P2 microparticle. However, when the same P2 inner core is surrounded by an outer shell formed with R10, whose swelling ratio is higher as  $0.31 \pm 0.13$ , the inner core increases almost three times to  $0.35 \pm 0.11$ . This indicates that the outer shell squeezes the inner shell while shrinking, and the shrinkage degree of the inner shell is further increased.

### 2.2.2. Nanoparticle Encapsulation

Most aqueous-dispersed materials are inadequate to be encapsulated inside the PNIPAm capsule by emulsion methods since

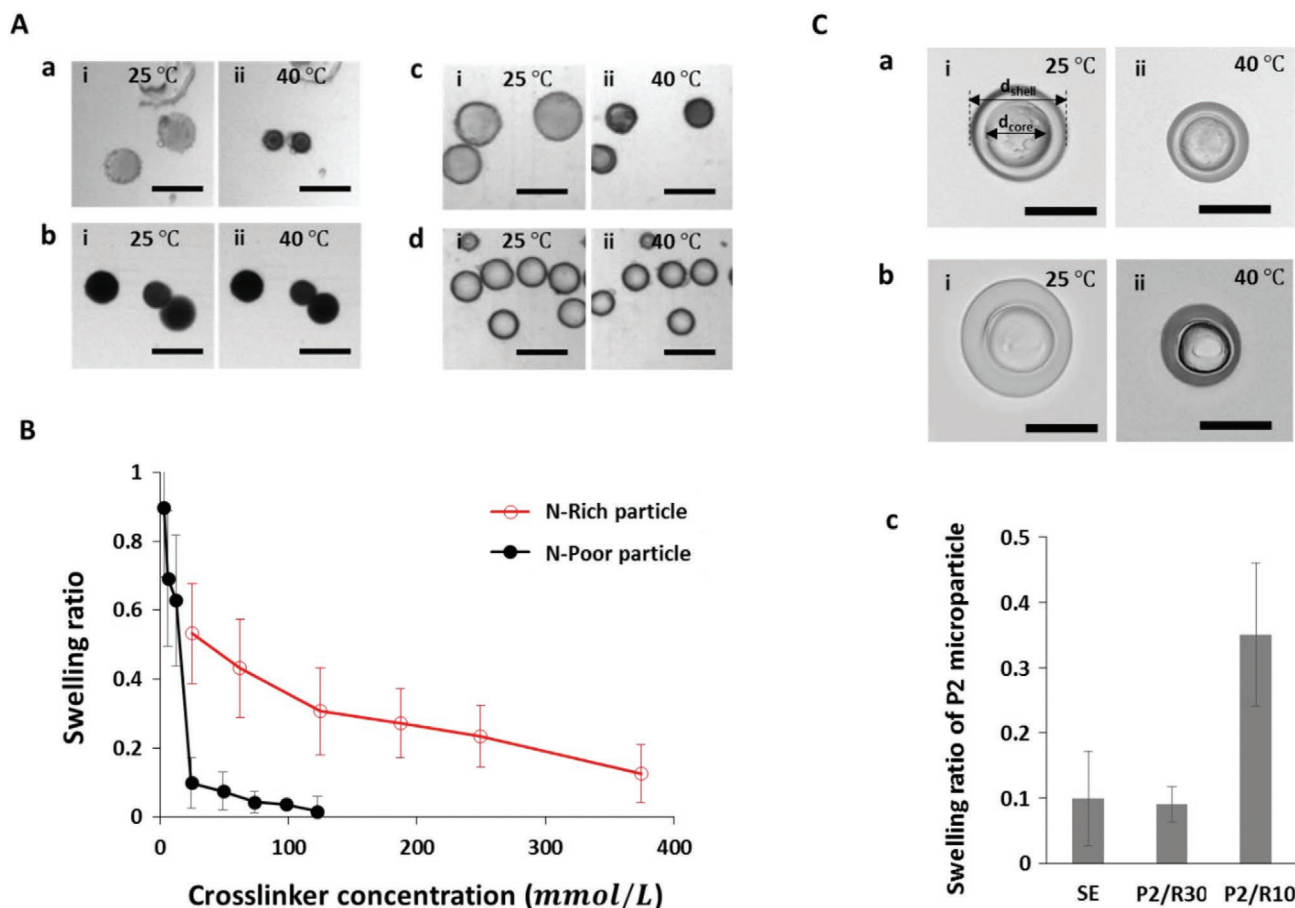


**Figure 2.** Effect of the degree of crosslinking on swelling behavior of microcapsules. A) Optical images of microparticles formed with a) P1, b) P2, c) R2, and d) R30 solutions for i) swollen at 25 °C and ii) shrunk state at 40 °C. The chemical composition of each solution is given in Table S1 in the Supporting Information. B) Variations in the linear swelling ratio of N-rich and N-poor microparticles as a function of the crosslinker concentration. C) Swelling characteristics of the TCGS microcapsule depending on the outer layer. Optical images of thermoresponsiveness of TCGS microcapsules a) core formed with P2 and shell formed with R30 and b) inner core with P2 and outer shell with R10. c) Comparison of swelling ratio of P2 microcapsule depending on outer layer condition. Scale bars: 50  $\mu\text{m}$ .

the precursor monomer solution of PNIPAM has a similar polarity to the encapsulated materials. Therefore, instead of encapsulation, the materials are loaded by diffusion or absorption after the formation of the PNIPAM capsules.<sup>[14b,23]</sup> This has limitations in the size of loaded materials, i.e., it should be smaller than the PNIPAM network. Our TCGS platform does not have the above limitation, and thereby aqueous-dispersed materials whose size is larger than the PNIPAM network can be encapsulated inside the capsule. This is possible by using an oleophilic N-rich monomer solution, which has opposite polarity with a core solution, as an outer shell material. To demonstrate this encapsulation, rhodamine-B-labeled polystyrene nanoparticles (110 nm in diameter) were added in the  $W_{n\text{-poor}}$  inner fluid (0.5% v/v), and TCGS microcapsules were generated (Figures S5 and S8, Supporting Information). The successful encapsulation of nanoparticles inside the polymer network was observed by a confocal microscope (Figure 3). Most of the particles were located in the space between the inner core and outer shells (Figure 3A; Figure S6, Supporting Information). Even if the volume of microcapsules suddenly changed as the temperature changed, the encapsulated nanoparticles remained

inside (Figure 3B). In Figure 3B, the brightness of the fluorescent intensity was increased with temperature, indicating that the particles are more densely packed inside the gap. At 25 °C, the relative fluorescence unit (RFU) across the middle of the capsule (dotted line from i to ii in Figure 3Ab, Bb) shows two peak values at the space between the inner core and outer shell (Figure 3C). As the temperature increased up to 40 °C and microcapsules shrunk, the peak values of RFU increased, and the peak locations of RFU became narrower than those at 25 °C. When integrating all normalized RFU values in the middle plane of the microcapsule, the normalized RFU of a single microcapsule increased. This indicates that particles stayed within microcapsules.

### 2.2.3. Dual Stimuli-Responsive Microcapsules

To further diversify the use of the microcapsules, the inner core or outer shell was chemically modified by incorporating itaconic acid (IA), a pH-responsive monomer. To investigate the pH-responsive effects, the microparticle was formed from single

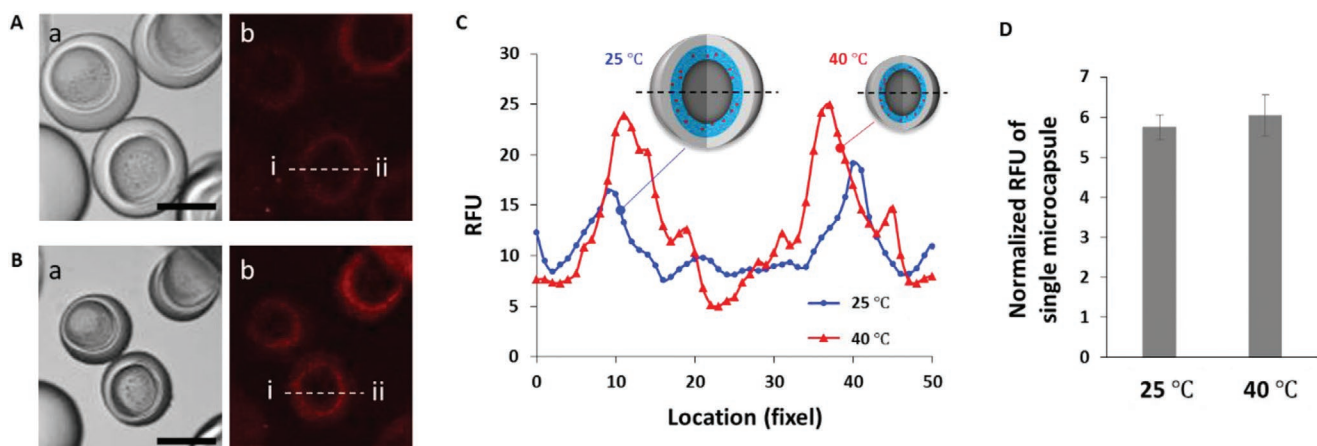


**Figure 3.** Nanoparticle encapsulation within the TCGS microcapsules. A) Rhodamine-B-labeled polystyrene nanoparticles are encapsulated within the TCGS microcapsules. a) Optical images and b) confocal microscope images of microcapsules encapsulating nanoparticles at A) 25 °C and B) 40 °C. C) Relative fluorescence unit (RFU) across the center of the microcapsules (dotted line from i to ii in Figure 3Ab, Bb) at different temperatures. D) Normalized RFU values of individual microcapsules at different temperatures. Scale bars: 50  $\mu\text{m}$ .

emulsion templates using 500  $\mu\text{L}$  of R5 solution containing 38  $\mu\text{mol}$  of itaconic acid, and designated P(NIPAm\_R5-co-IA). The equilibrium degree of swelling of the P(NIPAm\_R5-co-IA) microparticle varied depending on pH values, measured as  $0.71 \pm 0.09$ ,  $0.48 \pm 0.08$ , and  $0.38 \pm 0.06$  at pH 4, 7, and 10 of external solutions, respectively (Figure 4A). On the other hand, PNIPAm microparticles made with R5 solution, P(NIPAm)\_R5, showed an almost constant swelling ratio regardless of the pH of the

external solution. To investigate the effect of chemical modification of the inner core, microparticles were prepared using 500  $\mu\text{L}$  of P2 solution containing 38  $\mu\text{mol}$  of itaconic acid and named P(NIPAm\_P2-co-IA). The equilibrium degree of swelling of the P(NIPAm\_P2-co-IA) microparticles varied depending on pH values, measured as  $0.44 \pm 0.11$ ,  $0.14 \pm 0.05$ , and  $0.10 \pm 0.04$  at pH 4, 7, and 10 of external solutions, respectively (Figure 4B; Figure S7A, Supporting Information). Furthermore, it is expected that the

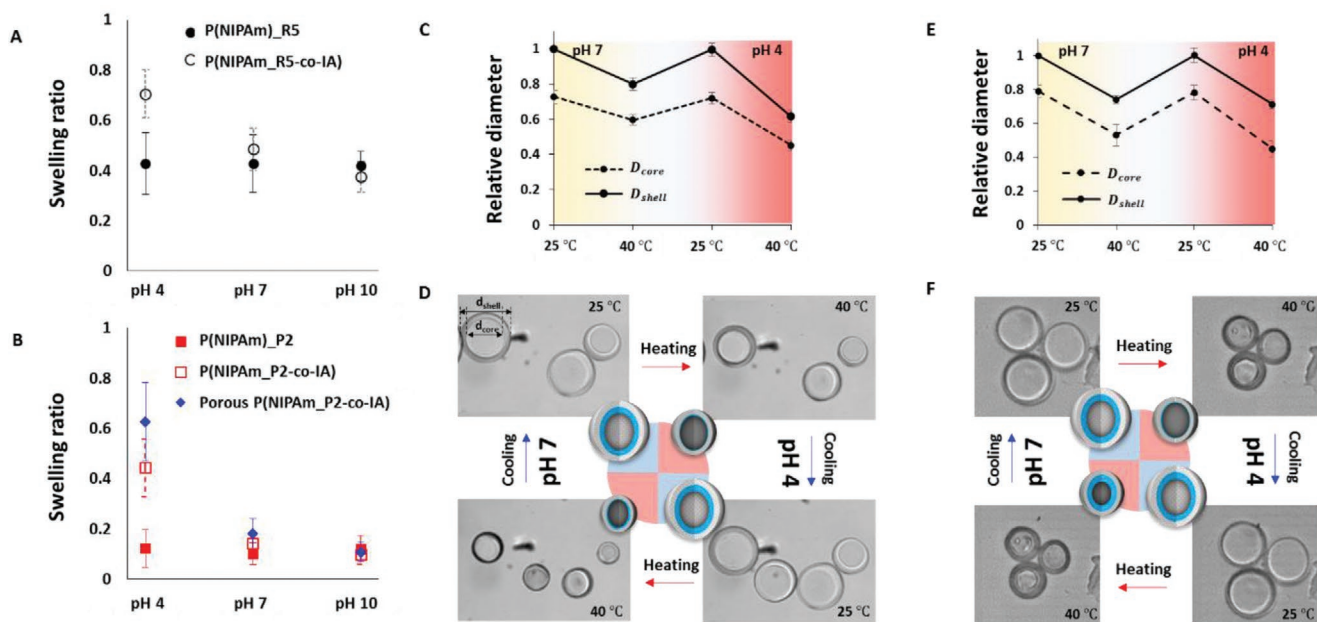


**Figure 4.** Dual stimuli-responsive microcapsule. A) Variation of the swelling ratio of PNIPAm\_R5 and P(NIPAm\_R5-co-IA) microparticles depending on pH of the external solution. B) Variation of the swelling ratio of PNIPAm\_P2, P(NIPAm\_P2-co-IA), and porous P(NIPAm\_P2-co-IA) microparticles depending on pH of the external solution. C) Relative diameter variations of the inner core and the outer shell of the shell-modified dual-responsive CGS microcapsule, the core of which consists of PNIPAm and shell of P(NIPAm\_R5-co-IA), as a function of pH and temperature. D) Optical images showing morphological variations of the shell-modified dual-responsive CGS microcapsule depending on pH and temperature. E) Relative diameter variations of the inner core and outer shell of the core-modified dual-responsive CGS microcapsule, the core of which is composed of P(NIPAm\_P2-co-IA) and shell of PNIPAm, as a function of pH and temperature. F) Optical images showing morphological variations of the dual-responsive CGS microcapsule depending on pH and temperature.

encapsulation of nanoparticles in the inner core will induce structural changes accordingly. To investigate the effect of the structural change, polystyrene nanoparticles (110 nm in diameter) were added in the pregel solution (0.5% v/v), and porous P(NIPAm-*P2-co-IA*) microparticles were also prepared. After single emulsion templates were polymerized and washed, porous microparticles composed of P(NIPAm-*co-IA*) were formed. Since the single microparticles were not surrounded by a shell, most of the nanoparticles were washed out of the hydrogel during the polymerization and washing process. The remaining network was a porous structure and consequently an increasing degree of volume change was observed.<sup>[14c,22]</sup> When the porous structures were added, the degree of swelling values was increased to  $0.62 \pm 0.15$ ,  $0.17 \pm 0.06$ , and  $0.11 \pm 0.04$  compared to the non-porous microparticles. Overall, the lower the pH, the greater the increase in the swelling ratio compared to PNIPAm. At pH 10, there is only a small difference in all cases due to the pH.

By using this P(NIPAm-*R5-co-IA*) hydrogel as the outer shell and P2 PNIPAm as the inner core, shell-modified CGS microcapsules with dual stimuli-responsiveness were produced (Figure 4C,D). During sequentially changing the temperature and pH of the external solution, the dual functionality of the microcapsule was demonstrated. In the beginning, the microcapsules were swollen at pH 7 and 25 °C external solution. Then, they were heated up to 40 °C and shrunk. The external solution was then carefully changed to a solution of pH 4, and the microcapsules were swollen again by cooling down to 25 °C. Afterward, the temperature was increased again up to 40 °C, and thereby microcapsules shrunk again. Finally, the external solution was again gradually changed to a solution of pH 7, and microcapsules were cooled to 25 °C and swollen. During the repetition of this cycle, the relative diameter of the inner core,  $D_{\text{core}} = \frac{d_{\text{core}}}{d_{\text{shell\_initial}}}$ , and the relative diameter of the outer shell,

$$D_{\text{shell}} = \frac{d_{\text{shell}}}{d_{\text{shell\_initial}}},$$

where  $d_{\text{core}}$ ,  $d_{\text{shell}}$ , and  $d_{\text{shell\_initial}}$  are defined as a diameter of the inner core, a diameter of the outer shell, and an initial diameter of the outer shell, respectively. As a result, both values of  $D_{\text{core}}$  and  $D_{\text{shell}}$  were decreased/increased by heating/cooling (Figure 4C). When swollen at 25 °C,  $D_{\text{core}}$  and  $D_{\text{shell}}$  reached similar values regardless of the pH of the solution. When the CGS microparticles were shrunk at 40 °C,  $D_{\text{shell}}$  values reached  $0.79 \pm 0.04$  and  $0.60 \pm 0.03$  at pH 7 and pH 4, respectively, which implies that the outer shell shrunk more in the lower pH solution. As the outer shell shrunk and compressed the inner core,  $D_{\text{core}}$  values at pH 4 ( $0.46 \pm 0.03$ ) is lower than that at pH 7 ( $0.60 \pm 0.03$ ). Material access to and from the outside was restricted, since the polymer network of the shell densified more under heated acidic conditions. Therefore, this CGS system with dual-responsiveness of the outer shell can serve as a gateway for the transport of molecules to and from the external solution.

By using the P(NIPAm-*P2-co-IA*) hydrogel as the inner core and R5 PNIPAm as the outer shell, core-modified dual stimuli-responsive CGS microcapsules were prepared (Figure 4E,F). When swollen at 25 °C,  $D_{\text{core}}$  and  $D_{\text{shell}}$  reached similar values regardless of the pH of the solution. When the CGS microparticles were shrunk at 40 °C,  $D_{\text{core}}$  values reached  $0.53 \pm 0.06$  and  $0.44 \pm 0.04$  at pH 7 and pH 4, respectively, which implies

the core shrunk more under heated and acidic condition than under neutral condition, while the shell size was not significantly affected by the pH concentration. Accordingly, the size of the gap space was controlled according to temperature and pH, which resulted in the chemical reaction within the gap being promoted or reduced. The chemical reaction, which changes the pH within the capsule, is an example for an application of this gap size regulation system. By enlarging/reducing the gap size due to the change in pH, the chemical reaction can be temporarily decelerated/accelerated. Although the peculiarity of the dual-responsive CGS system mainly appeared when both heating and acidic condition were given, the overall tendency is that the core and the shell of microcapsule can be individually modified and controlled by temperature and pH of the external solution.

### 2.3. Temperature-Controlled Enzymatic Reaction

As a practical application, we developed a thermocontrolled glucose sensor with the TCGS microcapsule platform. The GOX@nanocontainers whose diameter is about 400 nm were encapsulated inside the microcapsules but freely dispersed throughout the internal space between core and shell (Figure S9, Supporting Information).<sup>[24]</sup> Since the size of glucose molecules (180 Da; 8.5 Å), which are supplied from the external solution, is comparably smaller than the pore size of PNIPAm network, the glucose molecules can diffuse into the internal space through the outer shell, and the enzymatic reaction can proceed by trapped GOX@nanocontainers (Figure 5A). As GOX catalyzes, the conversion of glucose to gluconic acid and hydrogen peroxide, the enzymatic reaction can be quantitatively analyzed. Amplex red is converted to resorufin as it is oxidized by horseradish peroxidase (HRP) in the presence of hydrogen peroxide and consequently generated fluorescence with excitation at 555 nm and emission at 595 nm (Figure 5B inset). When investigating changes in the RFU generated by the reaction of the GOX@nanocontainers, RFU at 42 °C was almost 41% higher than that at 25 °C at the beginning of the reaction. 5 min after reaction started, RFU at 42 °C was still 21% higher on average than that at 25 °C. The reaction velocity of the GOX@nanocontainers was faster when the temperature was high (up to 42 °C) (Figure 5B).<sup>[25]</sup> In contrast to this general tendency, the GOX@nanocontainers in our thermocontrolled microcapsules showed opposite reaction behaviors in response to temperature. The reaction velocity at 42 °C was slower than that at 25 °C throughout the measurement (Figure 5C). More interestingly, the rapid increase of the initial velocity until 1.5 min was observed at 25 °C, and the increase rate gradually decreases. As the reaction proceeded, the products inhibited the enzyme activity. This is attributed to limited mass transport out of the shell. The feedback inhibition effect may influence the reaction more than the normal free-diffusion case, since the products are accumulated in the confined volume of the narrow gap of TCGS. Even after 1.5 min, the reaction velocity at 25 °C was still much faster than that at 42 °C. When comparing overall reaction activity of TCGS microcapsules encapsulating GOX@nanocontainers, GOX@nanocontainers, and native GOX, only our microcapsule model showed 40% less activity responding to temperature increase, while the other two

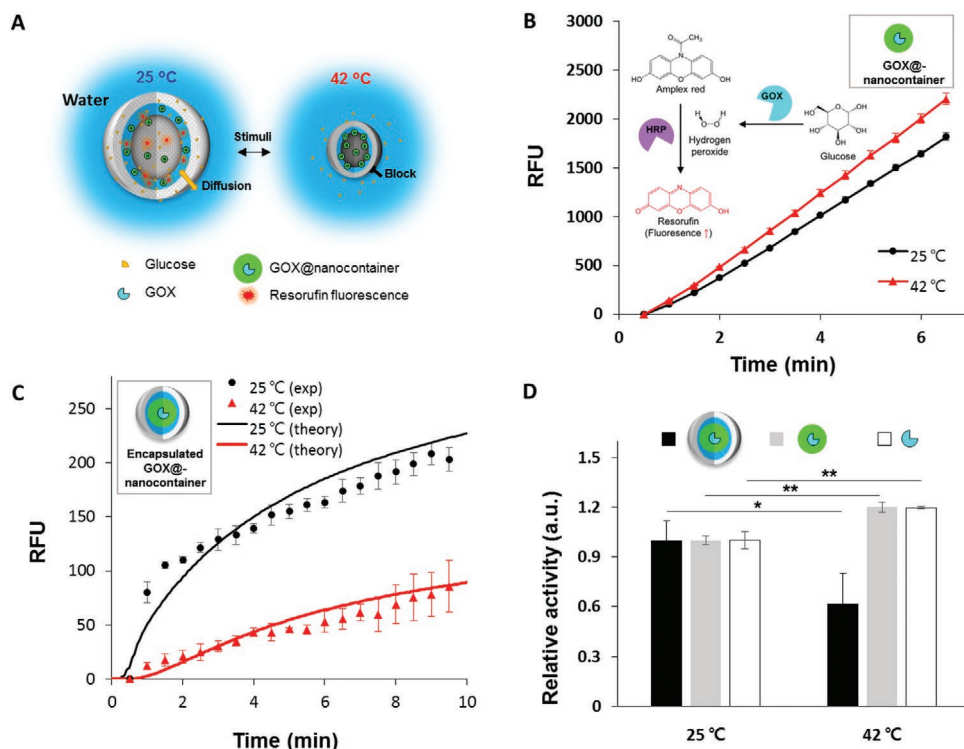


**Figure 5.** Temperature-controlled glucose sensor. A) Schematic diagram of the strategy for a thermo-controlled glucose sensor developed with TCGS microcapsules encapsulating GOX@nanocontainers. B) Reaction of GOX@nanocontainers at different temperature (25 and 42 °C). Inset describes the enzymatic assay of GOX. GOX catalyzes the production of hydrogen peroxide by the consumption of glucose, followed by HRP (peroxidase) and the hydrogen peroxide converts Amplex red to resorufin. C) Reaction of GOX@nanocontainers in TCGS microcapsules below and above LCST. D) Comparison of the total reaction rate of native GOX, bare GOX@nanocontainers, and GOX@nanocontainers in TCGS microcapsules from 1.5 to 9.5 min at a temperature of 25 and 42 °C (\**p* value < 0.1, \*\**p* value < 0.05; two-tailed *T*-test).

cases showed rather around 20% increased activity (Figure 5D). It provides compelling evidence that our PNIPAM microcapsule effectively controls glucose detection in a temperature-responsive manner.

In order to better understand the hypothetical mechanism of the enzymatic reaction throughout the TCGS microcapsule, we designed a mathematical model that predicts the diffusion-reaction behaviors. We assume that the TCGS microcapsule consists of homogeneous enveloping concentric layers, and has GOX@nanocontainers in the gap without diffusion to the core or the shell layer (Figure 6A). At  $t = 0$ , the TCGS microcapsule is placed in the cocktail solution, which contains influent reactants—glucose, Amplex red—and HRP, and these diffuse into each layer with the constant diffusivities. Assuming the reaction rate as  $k$ , we can obtain the following reaction-diffusion equations of glucose, Amplex red, and resorufin, the concentrations of which are denoted by  $c_g$ ,  $c_a$ , and  $c_r$ , respectively

$$\frac{\partial c_g(r,t)}{\partial t} = \frac{1}{r^2} \frac{\partial}{\partial r} \left[ D_g(r) r^2 \frac{\partial c_g(r,t)}{\partial r} \right] - k c_g(r,t) c_a(r,t) \quad (1)$$

$$\frac{\partial c_a(r,t)}{\partial t} = \frac{1}{r^2} \frac{\partial}{\partial r} \left[ D_a(r) r^2 \frac{\partial c_a(r,t)}{\partial r} \right] - k c_g(r,t) c_a(r,t) \quad (2)$$

$$\frac{\partial c_r(r,t)}{\partial t} = \frac{1}{r^2} \frac{\partial}{\partial r} \left[ D_r(r) r^2 \frac{\partial c_r(r,t)}{\partial r} \right] + k c_g(r,t) c_a(r,t) \quad (3)$$

$$D_g(r) = \begin{cases} D_g^c, & r < r_c \\ D_g^g, & r_c < r < r_g, D_a(r) = D_r(r) \\ D_g^s, & r_g < r < r_s \end{cases} \quad D_r(r) = \begin{cases} D_a^c, & r < r_c \\ D_a^g, & r_c < r < r_g \\ D_a^s, & r_g < r < r_s \end{cases} \quad (4)$$

with the initial condition as

$$c_g(r) = \begin{cases} c_g^0, & r > r_s \\ 0, & \text{elsewhere} \end{cases} \quad (5)$$

$$c_a(r) = \begin{cases} c_a^0, & r > r_s \\ 0, & \text{elsewhere} \end{cases} \quad (6)$$

$$c_r(r) = 0 \quad (7)$$

where symmetries in the zenith and the azimuth direction are assumed, and where  $r_c$ ,  $r_g$ , and  $r_s$  are radii of the core, gap, and shell, respectively.  $D_g$ ,  $D_a$ , and  $D_r$  denote the diffusion coefficients of glucose, Amplex red, and resorufin, and the parameters in each layer are taken as follows:  $D_g^g = D$ ,  $D^c = 0.2D$ ,  $D^s = 0.8D$  in the case of 25 °C and  $D^s = 0.2D$  in the case of 42 °C, where  $D$  is a diffusion coefficient in free aqueous solution. The lower diffusion constant in the shell  $D^s$  at higher temperatures is mainly due to the shrinkage of

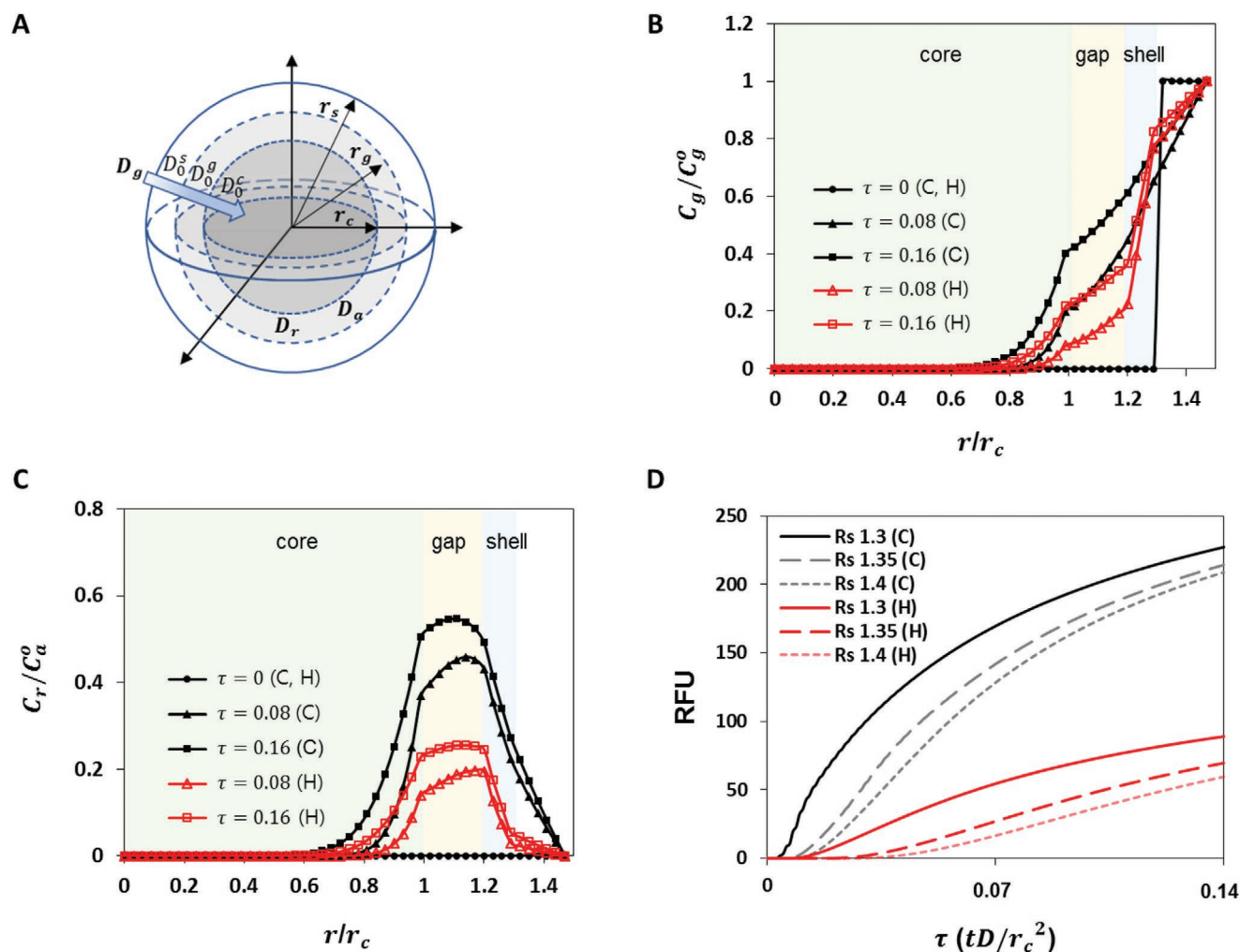


**Figure 6.** Numerical analysis of the diffusion-reaction process of a temperature-controlled glucose sensor. A) Schematic representation of the radially symmetrical TCGS microcapsule in a spherical coordinate. Concentration profiles for relative B) glucose and C) resorufin at different times and temperatures. The line C (black) and H (red) indicate the cooled and heated states in which the temperature is below or above LCST. D) Plot of RFU, normalized  $\sum c_r(r,t) \cdot 4\pi r^2 \cdot dr$ , over time with different shell thicknesses and temperatures.

the polymer networks. The reaction rate  $k$  is primarily determined by the activity of the enzymes, HRP and GOX. Since the enzymes are continuously reused with high turnover rate, we assumed that the diffusion effect of HRP was negligible. We assume that the reaction rate  $k$  decays with increasing reaction

$$k(t) = \begin{cases} \alpha \cdot k(0) / \exp(c_r(r,t)), & r_c < r < r_g \\ 0, & \text{elsewhere} \end{cases} \quad (8)$$

The temperature-dependent constant  $\alpha$  is assigned as 1 for the 25 °C case and as 1.2 for the 42 °C case, which is estimated from the experimental results in Figure 5B, where the slope of 42 °C case is 1.2 times greater than 25 °C case. The concentration values of the components are numerically solved in a truncated finite domain,  $0 < \frac{r}{r_c} < 1.5$ , where the regions of  $1 < \frac{r}{r_c} < 1.2$  and  $1.2 < \frac{r}{r_c} < 1.3$  are defined as the gap and the shell, respectively (Figure 6). The concentration of the glucose gradually decreased from the outside to the inside of the TCGS,

and its gradient changed rapidly at the interface of each layer where the diffusion coefficient changed (Figure 6B). The lower  $D^s$  at higher temperature resulted in lower glucose concentrations within the shell. On the other hand, the concentration of the resorufin  $c_r$  in the gap increased over time, and gradually spread out through the core and the shell (Figure 6C). In the early stage of the reaction, the resorufin concentration lowered toward the inside of the TCGS, and became almost symmetrical in the course of the reaction. RFU values are estimated by integrating the  $c_r$  inside the gap as  $RFU \approx \sum c_r(r,t) \cdot 4\pi r^2 \cdot dr$ , and the values upon different shell thickness,  $R_s = \frac{r_s}{r_c}$ , and different temperatures are displaced in Figure 6D. The slope of the RFU in Figure 6D gradually decreased with time. The thicker the shell, the longer the delay time for the first RFU to detect, because the influent chemicals need time to pass through the shell. The numerical results of the RFU show an excellent agreement with the experimental results (Figure 5C), indicating that the results correspond to our hypothetical mechanism of the diffusion coefficient variation with the temperature under

*k*-decaying condition. When the temperature is higher than LCST of PNIPAm, the GOX reaction is suppressed because a shrunken polymer network of the outer shell and the increase in the concentration of the inner solution inhibits the diffusion of incoming chemicals from outside into the gap. When the temperature is lowered below LCST, the glucose can easily diffuse into the capsule through a loose polymer network, which leads to an intensification of the reaction. In this way, glucose detection can be controlled on-demand in our thermocontrolled microcapsule system.

### 3. Conclusion

In summary, a one-step synthesis of stimuli-responsive microcapsules with temperature-responsive core–gap–shell structures for versatile design is introduced by a microfluidic approach in a simple and low risk manner. We can achieve the core–gap–shell structure with a double emulsion template, thereby reducing the risk of instability in higher-order emulsions. Moreover, our approach to produce temperature-responsive core–gap–shell microcapsules might allow larger scale production as our platform does not require the surface treatment procedure that is normally needed for a partially hydrophilic channel. However, this requires excellent control of microchannel geometry, wettability, as well as flow rates. The design variability of the microcapsules was demonstrated by individually controlling the water absorption ability of the inner core and outer shell. In addition, a free-radical polymerization with pH-responsive itaconic acid at the inner core or the outer shell of the capsule resulted in a poly(NIPAm-co-itaconic acid)(P(NIPAm-co-IA)), which has dual-responsiveness. As the pH-responsive polymer is engineered in this study, the inner core and outer shells of microcapsules can be individually designed with diverse stimuli-responsive materials, such as light-responsive and magnetic-responsive. Furthermore, polystyrene nanoparticles and GOX@nanocontainers were directly loaded inside the cavity during the formation of the microcapsules, and controlled enzymatic reaction was successfully demonstrated. It would be practically beneficial in mass production of chemicals, which can be controlled by simply changing the temperature, and not by the addition of inhibitors. In the future, the proposed TCGS microcapsule with stimuli-responsiveness will provide more practical applications by incorporating various bioactive compounds.

### 4. Experimental Section

**Pregel Solution Preparation:** The N-rich and N-poor phase solutions were prepared by dissolving 1 g of NIPAm (Sigma-Aldrich) in 1 mL of distilled water. The supersaturated NIPAm solution was maintained at 25 °C for about 20 min until the phase separation was complete. After two phases were fully separated into supernatant N-rich solution and substratum N-poor solution, 500 µL of each phase was carefully extracted. To prepare  $W_{n-rich}$  and  $W_{n-poor}$  pregel solutions, MBAm (Sigma-Aldrich, Germany) and 2-hydroxy-4'-(2-hydroxyethoxy)-2-methylpropiophenone (Irgacure 2959; Sigma-Aldrich, Germany) were added as crosslinker and photoinitiator, respectively, into each of the N-rich and the N-poor phase solutions. The amount of MBAm in the solution was adjusted from 1.62 to 194.59 µmol to vary the degree of crosslinking while the amount of Irgacure 2959 was maintained at

35.7 µmol (Table S1, Supporting Information). As surfactant in N-poor solution, 0.28% w/v of PF-127 was used, which is below the critical micelle concentration (CMC) of PF-127 (0.35% w/v) and PF-127 is mostly present in the unimer form.<sup>[26]</sup> Since the N-rich solution has the oleophilic property, 5% v/v of Span 80 (Sigma-Aldrich, Germany), which is a lipophilic emulsifier with HLB of 4.3, was used as surfactant in N-rich solutions. Silicon oil (20 cst, Sigma-Aldrich, Germany) with 5% v/v DC749 (Dow Corning GmbH, Germany) was used as a continuous fluid and collection solution.

**Microfluidic Generation of Double Emulsions:** Polydimethylsiloxane-based microfluidic device was used for generating double emulsion droplets as templates for the synthesis of the microcapsules. For generating the  $W_{n-poor}/W_{n-rich}/O$  double emulsions, pregel solutions of  $W_{n-poor}$  and  $W_{n-rich}$  were injected into a microfluidic device by pneumatic pressure controller (OB1, Elveflow) as inner fluid and middle fluid, respectively. The induced pressures at  $W_{n-poor}$ ,  $W_{n-rich}$ , and O phases were ≈120, 120, and 200 mbar, respectively. The formation process of double emulsions was monitored by using an inverted optical microscope (Leica DMI8) equipped with a high-speed CMOS camera (Vision research, Phantom v1610). Right after being collected in the collection solution, the double emulsions were converted into TCGS microcapsules under UV irradiation (310–390 nm, UVICO, Rapp OptoElectronic GmbH). To remove the outer oil solution, the microcapsules were washed several times with isopropanol and distilled water. Afterward, the microcapsules were stored in distilled water, so that they were fully hydrated and excess reactants could be dissolved out.

**Preparation of Polystyrene Nanoparticles:** Fluorescently labeled polystyrene nanoparticles were prepared by direct miniemulsion.<sup>[27]</sup> All chemicals were purchased from Sigma-Aldrich (Germany). First, a monomer mixture was prepared by combining styrene (98.9 mol%), divinylbenzene (1 mol%), and rhodamine B methacrylate (0.1 mol%). Styrene and divinylbenzene were purified on a column of basic aluminum oxide. Then, 0.25 g of hexadecane and 27.6 mg of 2,2'-azobis(2-methylbutyronitrile), which was recrystallized in MeOH, were added to 3 g of the monomer mixture. This organic phase was mixed with 24 g of an aqueous solution of Lutensol AT50 (1.4 wt%). The biphasic mixture was emulsified by microfluidization (75 µm Y chamber, 10 000 PSI, 3 cycles). The suspension was polymerized by immersing the samples in an oil bath at 72 °C overnight. After polymerization, the nanoparticles were purified by dialysis against a solution of Lutensol AT-50 (0.02 wt%), and the final surface tension of the suspension was 60 mN m<sup>-1</sup>.

**Preparation of GOX@nanocontainers:** Glucose oxidase from *Aspergillus niger* Type X-5 (GOX; EC. 1.1.3.4, 149 unit mg<sup>-1</sup>), D-(+)-glucose (a mixture of  $\alpha$  and  $\beta$  anomers), Amplex red (Ampliflu Red), tetraethyl orthosilicate (TEOS), 3-aminopropyl trimethoxysilane (APTMS), potassium fluoride, and toluene were purchased from Sigma-Aldrich (St. Louis, MO, USA). HRP (EC. 1.11.1.7, 300 unit mg<sup>-1</sup>), NHS-fluorescein, and dextran desalting column were provided by Thermo Scientific (Waltham, Massachusetts, USA). *n*-Hexanol was obtained from Carl Roth (Karlsruhe, Germany). Polyglycerol polyricinoleate (PGPR) was kindly gifted from Danisco (Copenhagen, Denmark). Lutensol AT50 was purchased from BASF (Ludwigshafen, Germany).

Silica nanocontainers with loaded GOX (GOX@nanocontainers) were prepared by following a previous report.<sup>[23]</sup> A water-in-oil (W/O) miniemulsion was prepared from a mixture of toluene (1.5 mL), PGPR (14 mg), and TEOS (32 µL) as a continuous phase, and APTMS (5.4 µL), potassium fluoride, and fluorescein-labeled GOX in sodium phosphate buffer ( $40 \times 10^{-3}$  M, pH 7.4) as an aqueous phase (50 µL). Emulsification was performed using a tip-type sonicator. After 24 h reaction at ambient temperature, the resultant was purified by centrifugation, and redispersed in 0.5 w/v % Lutensol AT-50 solution. Size distribution of the nanocontainers was measured by a Zetasizer (Malvern, United Kingdom). The morphology of the nanocontainers was observed by a JEM1400 (JEOL, Japan).

GOX (4 mg) was reacted with 16 excessive molar amount of NHS-fluorescein (0.19 mg). The NHS-fluorescein solution in dimethyl sulfoxide (2.5 µL) was added to reaction buffer (500 µL, pH 7.4,  $10 \times 10^{-3}$  M phosphate buffer) with GOX. After 1 h reaction, the resulting solution was passed through a dextran desalting column to remove unreacted

dye. The labeled GOX was adjusted to 4 mg mL<sup>-1</sup> solution. Bradford assay was used to determine the GOX.

**Enzymatic Assay for GOX:** A reaction cocktail was constituted as follows: phosphate buffer (0.9 mL, 10 × 10<sup>-3</sup> M, and pH 7.4), glucose solution (50 μL, 100 × 10<sup>-3</sup> M), HRP solution (50 μL, 100 unit mL<sup>-1</sup>), and Amplex red (3 μL, 1 × 10<sup>-3</sup> M in DMSO).<sup>[24]</sup> For GOX assay, the reaction cocktail was put into 96-well plate, and temperature was adjusted to 25 or 42 °C by a TECAN plate reader (Infinite M1000, Tecan Group Ltd., Männedorf, Switzerland). To initiate reaction, the enzyme sample (5 μL) was added to the reaction cocktail and the changes were monitored in fluorescence (excitation 555 nm/emission 595 nm) at intervals of 30 s by the TECAN plate reader.

**Characterization:** Fluorescence-labeled nanoparticles embedded inside the microcapsules were imaged by inverted confocal laser scanning microscope (Olympus IX81 FluoView 1000, Germany) with a 20× objective lens, and images were analyzed using FV10-ASW 4.2 viewer software (Olympus, Germany) and ImageJ 1.48v (Wayne Rasband, National Institutes of Health, USA).

Linear swelling ratio is defined by the equation of  $\frac{d_{25\text{ °C}} - d_{40\text{ °C}}}{d_{40\text{ °C}}}$ , where  $d_T$  is the diameter of the microcapsule at the certain temperature  $T$ . Normalized RFU is defined as  $\frac{I_a}{I_{\max} - I_{\min}}$ , where  $I_a$  indicates the measured RFU value at the pixel position of  $a$ , and  $I_{\min}$  and  $I_{\max}$  are the minimum and maximum RFU values inside the field of view, respectively. Normalized RFU of single microcapsules is the summation of all normalized RFU values inside the microcapsules.

## Supporting Information

Supporting Information is available from the Wiley Online Library or from the author.

## Acknowledgements

The authors thank the Volkswagen Foundation Initiative LIFE (Project Living Foam) and the MaxSynBio Consortium which is jointly funded by the Federal Ministry of Education and Research of Germany and the Max Planck Society.

Open access funding enabled and organized by Projekt DEAL.

## Conflict of Interest

The authors declare no conflict of interest.

## Keywords

double emulsions, droplet microfluidics, encapsulation, enzymatic reaction, poly(*N*-isopropylacrylamide)

Received: July 16, 2020

Revised: August 25, 2020

Published online:

- [1] a) W. Li, L. Zhang, X. Ge, B. Xu, W. Zhang, L. Qu, C.-H. Choi, J. Xu, A. Zhang, H. Lee, *Chem. Soc. Rev.* **2018**, *47*, 5646; b) C. L. Mou, W. Wang, Z. L. Li, X. J. Ju, R. Xie, N. N. Deng, J. Wei, Z. Liu, L. Y. Chu, *Adv. Sci.* **2018**, *5*, 1700960; c) Y. Zheng, Z. Yu, R. M. Parker, Y. Wu, C. Abell, O. A. Scherman, *Nat. Commun.* **2014**, *5*, 5772; d) T. Y. Lee, T. M. Choi, T. S. Shim, R. A. Frijns, S.-H. Kim, *Lab Chip* **2016**, *16*, 3415; e) S. Nagelberg, L. D. Zarzar, N. Nicolas, K. Subramanian,

- J. A. Kalow, V. Sresht, D. Blankschtein, G. Barbastathis, M. Kreysing, T. M. Swager, *Nat. Commun.* **2017**, *8*, 14673.
- [2] a) F. He, M. J. Zhang, W. Wang, Q. W. Cai, Y. Y. Su, Z. Liu, Y. Faraj, X. J. Ju, R. Xie, L. Y. Chu, *Adv. Mater. Technol.* **2019**, *4*, 1800687; b) S. Neethirajan, I. Kobayashi, M. Nakajima, D. Wu, S. Nandagopal, F. Lin, *Lab Chip* **2011**, *11*, 1574; c) A. Abate, D. Weitz, *Small* **2009**, *5*, 2030; d) B. F. Silva, C. Rodríguez-Abreu, N. Vilanova, *Curr. Opin. Colloid Interface Sci.* **2016**, *25*, 98; e) I. J. Joye, D. J. McClements, *Curr. Opin. Colloid Interface Sci.* **2014**, *19*, 417; f) E. Dickinson, *Trends Food Sci. Technol.* **2012**, *24*, 4; g) H. M. Shewan, J. R. Stokes, *J. Food Eng.* **2013**, *119*, 781; h) S. Yang, F. Guo, B. Kiraly, X. Mao, M. Lu, K. W. Leong, T. J. Huang, *Lab Chip* **2012**, *12*, 2097.
- [3] M. Weiss, J. P. Frohnmayer, L. T. Benk, B. Haller, J.-W. Janiesch, T. Heitkamp, M. Börsch, R. B. Lira, R. Dimova, R. Lipowsky, *Nat. Mater.* **2018**, *17*, 89.
- [4] M. A. Zieringer, N. J. Carroll, A. Abbaspourrad, S. A. Koehler, D. A. Weitz, *Small* **2015**, *11*, 2903.
- [5] X. Xie, W. Zhang, A. Abbaspourrad, J. Ahn, A. Bader, S. Bose, A. Vegas, J. Lin, J. Tao, T. Hang, *Nano Lett.* **2017**, *17*, 2015.
- [6] C. Nam, J. Yoon, S. A. Ryu, C.-H. Choi, H. Lee, *ACS Appl. Mater. Interfaces* **2018**, *10*, 40366.
- [7] H. Lee, C. H. Choi, A. Abbaspourrad, C. Wesner, M. Caggioni, T. Zhu, S. Nawar, D. A. Weitz, *Adv. Mater.* **2016**, *28*, 8425.
- [8] a) Y. Cong, Q. Li, M. Chen, L. Wu, *Angew. Chem., Int. Ed.* **2017**, *56*, 3552; b) J. G. Werner, B. T. Deveney, S. Nawar, D. A. Weitz, *Adv. Funct. Mater.* **2018**, *28*, 1803385; c) J. G. Werner, S. Nawar, A. A. Solovev, D. A. Weitz, *Macromolecules* **2018**, *51*, 5798.
- [9] P. S. Clegg, J. W. Tavacoli, P. J. Wilde, *Soft Matter* **2016**, *12*, 998.
- [10] a) E. Amstad, M. Chemama, M. Eggersdorfer, L. R. Arriaga, M. P. Brenner, D. A. Weitz, *Lab Chip* **2016**, *16*, 4163; b) S. Akbari, T. Pirbodaghi, R. D. Kamm, P. T. Hammond, *Lab Chip* **2017**, *17*, 2067; c) E. Amstad, S. S. Datta, D. Weitz, *Lab Chip* **2014**, *14*, 705.
- [11] a) M. Windbergs, Y. Zhao, J. Heyman, D. A. Weitz, *J. Am. Chem. Soc.* **2013**, *135*, 7933; b) L. Y. Chu, T. Yamaguchi, *Adv. Mater.* **2002**, *14*, 386; c) J. Wei, X. J. Ju, X. Y. Zou, R. Xie, W. Wang, Y. M. Liu, L. Y. Chu, *Adv. Funct. Mater.* **2014**, *24*, 3312; d) Y. Chen, W. Wei, Y. Zhu, J. Luo, R. Liu, X. Liu, *ACS Appl. Mater. Interfaces* **2020**, *12*, 4821.
- [12] B. J. Sun, H. C. Shum, C. Holtze, D. A. Weitz, *ACS Appl. Mater. Interfaces* **2010**, *2*, 3411.
- [13] a) H. Zhu, S. Nawar, J. G. Werner, J. Liu, G. Huang, Y. Mei, D. A. Weitz, A. A. Solovev, *J. Phys.: Condens. Matter* **2019**, *31*, 214004; b) J. Liu, H. Chen, X. Shi, S. Nawar, J. G. Werner, G. Huang, M. Ye, D. A. Weitz, A. A. Solovev, Y. Mei, *Environ. Sci.: Nano* **2020**, *7*, 656.
- [14] a) B. Kim, H. S. Lee, J. Kim, S.-H. Kim, *Chem. Commun.* **2013**, 49, 1865; b) S. Seiffert, J. Thiele, A. R. Abate, D. A. Weitz, *J. Am. Chem. Soc.* **2010**, *132*, 6606; c) J. W. Kim, A. S. Utada, A. Fernández-Nieves, Z. Hu, D. A. Weitz, *Angew. Chem., Int. Ed.* **2007**, *46*, 1819; d) L. Liu, W. Wang, X.-J. Ju, R. Xie, L.-Y. Chu, *Soft Matter* **2010**, *6*, 3759.
- [15] a) C. Yang, R. Xie, W.-G. Liang, X.-J. Ju, W. Wang, M.-J. Zhang, Z. Liu, L.-Y. Chu, *J. Mater. Sci.* **2014**, *49*, 6862; b) S.-W. Pi, X.-J. Ju, H.-G. Wu, R. Xie, L.-Y. Chu, *J. Colloid Interface Sci.* **2010**, *349*, 512; c) H. Shibata, Y. J. Heo, T. Okitsu, Y. Matsunaga, T. Kawanishi, S. Takeuchi, *Proc. Natl. Acad. Sci. USA* **2010**, *107*, 17894; d) M.-J. Zhang, W. Wang, R. Xie, X.-J. Ju, L. Liu, Y.-Y. Gu, L.-Y. Chu, *Soft Matter* **2013**, *9*, 4150; e) Y.-M. Liu, X.-J. Ju, Y. Xin, W.-C. Zheng, W. Wang, J. Wei, R. Xie, Z. Liu, L.-Y. Chu, *ACS Appl. Mater. Interfaces* **2014**, *6*, 9530; f) X.-H. Ge, J.-P. Huang, J.-H. Xu, G.-S. Luo, *Lab Chip* **2014**, *14*, 4451; g) T. Kanai, D. Lee, H. C. Shum, R. K. Shah, D. A. Weitz, *Adv. Mater.* **2010**, *22*, 4998.
- [16] a) Y.-L. Yu, M.-J. Zhang, R. Xie, X.-J. Ju, J.-Y. Wang, S.-W. Pi, L.-Y. Chu, *J. Colloid Interface Sci.* **2012**, *376*, 97; b) W.-C. Jeong, S.-H. Kim, S.-M. Yang, *ACS Appl. Mater. Interfaces* **2014**, *6*, 826.

- [17] a) S. Sasaki, S. Okabe, Y. Miyahara, *J. Phys. Chem. B* **2010**, *114*, 14995; b) K. D. Seo, J. Doh, D. S. Kim, *Langmuir* **2013**, *29*, 15137.
- [18] S. Sasaki, *J. Phys. Chem. B* **2016**, *120*, 184.
- [19] a) N. Pannacci, H. Bruus, D. Bartolo, I. Etchart, T. Lockhart, Y. Hennequin, H. Willaime, P. Tabeling, *Phys. Rev. Lett.* **2008**, *101*, 164502; b) J. Guzowski, P. M. Korczyk, S. Jakiela, P. Garstecki, *Soft Matter* **2012**, *8*, 7269.
- [20] L. D. Zarzar, V. Sresht, E. M. Sletten, J. A. Kalow, D. Blankschtein, T. M. Swager, *Nature* **2015**, *518*, 520.
- [21] D. Guzey, D. J. McClements, *Adv. Colloid Interface Sci.* **2006**, *128*, 227.
- [22] H. Senff, W. Richtering, *Colloid Polym. Sci.* **2000**, *278*, 830.
- [23] R.-C. Luo, S. Ranjan, Y. Zhang, C.-H. Chen, *Chem. Commun.* **2013**, *49*, 7887.
- [24] S.-M. Jo, F. R. Wurm, K. Landfester, *Nano Lett.* **2019**, *20*, 526.
- [25] L. Chen, Z.-Q. Wu, C. Wang, J. Ouyang, X.-H. Xia, *Anal. Methods* **2012**, *4*, 2831.
- [26] a) C. Alvarez-Lorenzo, A. Sosnik, A. Concheiro, *Curr. Drug Targets* **2011**, *12*, 1112; b) A. Pitto-Barry, N. P. Barry, *Polym. Chem.* **2014**, *5*, 3291; c) G. Gyulai, A. Magyar, J. Rohonczy, J. Orosz, M. Yamasaki, S. Bősze, É. Kiss, *eXPRESS Polym. Lett.* **2016**, *10*, 216; d) M. Di Biase, P. de Leonadis, V. Castelletto, I. W. Hamley, B. Derby, N. Tirelli, *Soft Matter* **2011**, *7*, 4928.
- [27] K. Landfester, N. Bechthold, F. Tiarks, M. Antonietti, *Macromolecules* **1999**, *32*, 5222.